

High Responsivity, Low Dark Current Ultraviolet Photodetectors Based on Two-Dimensional Electron Gas Interdigitated Transducers

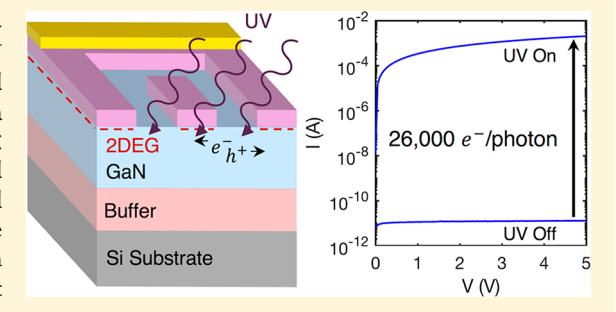
Peter F. Satterthwaite, †,‡ Ananth Saran Yalamarthy, †,‡,§ Noah A. Scandrette, A. K. M. Newaz, and Debbie G. Senesky*,†, _

Departments of †Electrical Engineering, §Mechanical Engineering, and ^LAeronautics and Astronautics, Stanford University, Stanford, California 94305, United States

Department of Physics and Astronomy, San Francisco State University, San Francisco, California 94132, United States

Supporting Information

ABSTRACT: An ultraviolet (UV) photodetector employing the twodimensional electron gas (2DEG) formed at the AlGaN/GaN interface as an interdigitated transducer (IDT) is characterized under optical stimulus. The 2DEG-IDT photodetector exhibits a record high normalized photocurrent-to-dark current ratio of 6 × 10¹⁴. We also observe a high responsivity (7800 A/W) and ultraviolet-visible rejection ratio (106), among the highest reported values for any GaN photodetector architecture. We argue that the valence band offset in the AlGaN/GaN heterostructure is essential in achieving this high responsivity, allowing for large gains without necessitating the presence of trap states. Our proposed gain



mechanism is consistent with measurements of the scaling of gain with device channel width and incident power. The photodetector architecture has a simple two-step fabrication process, compatible with AlGaN/GaN high electron mobility transistor (HEMT) processing. This unique combination of low dark current, high responsivity, and simple fabrication is attractive for a variety of UV sensing applications.

KEYWORDS: ultraviolet, photodetector, gain, responsivity, dark current, III-nitride semiconductor

TV photodetectors have applications in diverse fields, including combustion flame detection, UV astronomy, and satellite positioning. 1,2 GaN is an appealing materials platform for manufacturing UV photodetectors due to the maturity of GaN high electron mobility transistor (HEMT) fabrication technology, extensive research into next-generation nanostructured GaN optoelectronic devices,³ and the ability of GaN to operate in high-temperature and radiation-rich environments.4 Recent work has shown that III-nitride devices can even enable detection in the vacuum UV regime (<200 nm). In most applications, the ideal photodetector would exhibit a high responsivity to maximize the signal, in addition to a low dark current to minimize quiescent power. A performance metric which simultaneously captures these two values is the normalized photocurrent-to-dark current ratio (NPDR), defined as the ratio of responsivity to dark current, with units of 1/W.8,9 Numerous photodetector architectures^{2,10-18} have been demonstrated in GaN, with a broad range of reported responsivities and NPDRs, as summarized in Table 1. Table 1 additionally reports the UV-visible rejectionratio, another important performance metric that determines the cross-sensitivity of the photodetector to visible light. A distinction can be drawn between devices with a responsivity that corresponds to less than 100% quantum efficiency^{11,12} (0.29 A/W for 365 nm illumination) and those with a responsivity that exceeds this value. 16,13-17 In the latter

category of photodetectors, which includes photoconductors, 14 phototransistors, ^{13,19} and some metal–semiconductor–metal (MSM) photodetectors, ^{10,20} an internal gain mechanism must exist where each incident photon induces more than one electron in the conduction band. The gain (*G*) is defined as the ratio of charge carriers to the photon flux:

$$G = \frac{hc}{e\lambda} \frac{I}{P} \tag{1}$$

where I is the photocurrent, λ is the wavelength of incident radiation, and P is the incident power. One particularly high gain photodetector architecture is the phototransistor; AlGaN/ GaN phototransistors have been shown to achieve gains as high as 170000.¹³ Though these devices have a high gain, their fabrication requires the use of both n-and p-doped GaN. 13 Due to the high activation energies of all known acceptor-type dopants in GaN,²² it is desirable to fabricate photodetectors which do not require doping. It is further desirable to fabricate devices compatible with HEMT fabrication, in order to leverage mature GaN technology and enable monolithic integration. Previous HEMT photodetectors, 15,23 which leverage the modulation of the AlGaN/GaN 2DEG sheet

Received: August 22, 2018 Published: October 1, 2018



detector type	responsivity (A/W)	NPDR (1/W)	UV/vis rejection ratio	bias voltage (V)	refs
MSM	3.1	3×10^{12}	10 ⁵	10	Chang et al. ¹⁰
p-i-n diode	0.15	2×10^{9}	10^{3}	10	Xu et al. ¹¹
avalanche	0.13	2×10^{10}	10^4	20	Tut et al. ¹²
phototransistor	50000	5×10^{14}	10^{8}	3	Yang et al. ¹³
photoconductor	13000	4×10^{8}	10^{2}	1	Liu et al. ¹⁴
HEMT	3000	2×10^{6}	10^{3}	10	Khan et al. ¹⁵
meander	10000	8×10^{12}	10^4	5	Martens et al. ¹⁶
sliced-HEMT	33	1×10^{12}	10^{3}	5	Kumar et al. ¹⁷
2DEG IDT	7800	6×10^{14}	10^{6}	5	This Work

density under UV illumination, have been shown to have a high gain, however such devices also necessarily have high dark current, leading to some of the lowest NPDRs among reported devices (~10⁶). Recent work 16,17 has shown that, by introducing an intrinsic GaN channel between two 2DEG electrodes, a high NPDR can be achieved. Understanding the gain mechanism of such photodetectors is important for maturing this promising class of devices.

In this work, we present such a device with a record high NPDR (6×10^{14}) . In addition, the device has a responsivity (7800 A/W), and UV-visible rejection-ratio (10^6) that are among the highest reported values. We propose that our device has a similar gain mechanism to that of a phototransistor, in a device architecture that is significantly simpler to fabricate, requiring two masks and no doping. Evidence for this gain mechanism is provided by investigating the scaling of gain with channel length and incident power.

Devices were fabricated on an AlGaN/GaN-on-Si wafer (DOWA, Inc.) grown by metal—organic chemical vapor deposition (MOCVD). The III-nitride stack, illustrated schematically in Figure 1a, consists of a 1.5 μ m thick strain

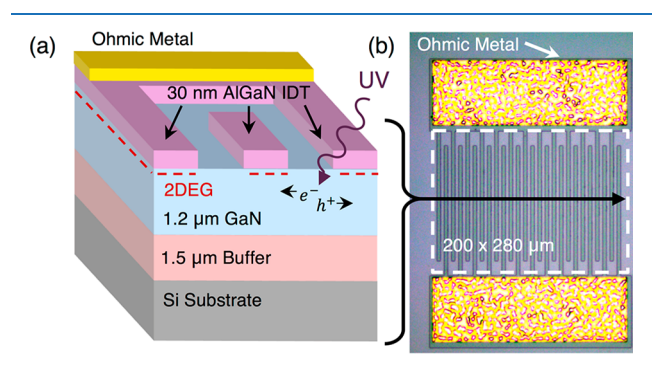


Figure 1. (a) Schematic illustration of the material stack. (b) Optical microscope image of the fabricated device.

management buffer structure and an active 1.2 μ m thick GaN layer grown on top of Si (111). Subsequent to the growth of the GaN layer, formation of the 2DEG was accomplished by growing an epitaxial stack consisting of a 1 nm-thick AlN spacer, 30 nm-thick $Al_{0.25}Ga_{0.75}N$ barrier layer and 1 nm-thick GaN capping layer. This wafer has a manufacturer-specified 2DEG mobility of $1400 \text{ cm}^2/\text{V}$ -s and sheet density of $1 \times 10^{13} \text{ cm}^{-2}$ at room temperature. As shown in Figure 1b, an array of 2DEG interdigitated transducers (2DEG-IDT) was fabricated by etching AlGaN 2DEG mesa electrodes. The mesa etch was performed using an inductive coupled plasma with BCl₃/Cl₂ gases to a depth of \sim 60 nm. These 5 μ m wide 2DEG electrodes were separated by 5 μ m wide intrinsic (uninten-

tionally doped below $10^{16}~\rm cm^{-3})$ GaN buffer channels. Post mesa isolation, a standard Ti/Al/Pt/Au Ohmic metal stack was deposited, and activated with a 35 s, 850 °C anneal. After this two-step process, the fabrication of the 2DEG IDT photodetectors was completed; however, it should be noted that the wafer received subsequent processing for cofabricated devices. In particular, standard MSM photodetectors were fabricated on the GaN buffer using the same geometry as the 2DEG-IDT photodetectors. These devices (Pd-MSM) had Pd/Au (40 nm/10 nm) metal fingers in place of the AlGaN mesa electrodes for comparison studies.

Responsivity measurements were taken using a 365 nm UV lamp and semiconductor parameter analyzer (henceforth Setup I). All presented measurements were taken at room temperature. The results of these measurements for a characteristic 2DEG-IDT and Pd-MSM device under 1.5 mW/cm² optical power are shown in Figure 2a. While both devices have a comparable, low dark current of ~10 pA, the 2DEG-IDT device has significantly higher photocurrent corresponding to a responsivity of 2500 A/W at 5 V, in contrast to the 0.78 A/W responsivity observed in the MSM photodetector at the same bias voltage. Though the 2DEG-IDT device has significantly higher responsivity, both devices have a responsivity that exceeds the 100% quantum efficiency limit (0.29 A/W for 365 nm illumination), indicating the presence of a gain mechanism in both devices.

To further probe the gain mechanism in the 2DEG-IDT device, we measured responsivity while varying the UV intensity across 4 orders of magnitude. These measurements are presented in Figure 2b. Measurements with incident power above 0.010 mW/cm² were DC measurements performed with Setup I, and those with power below 0.010 mW/cm² were AC measurements, performed using a lock-in amplifier and a monochromated optical beam chopped at 200 Hz (henceforth, Setup II). These data show that, as power increases from 0.15 to 110 μ W/cm², the responsivity increases dramatically by greater than 4 orders of magnitude, peaking at 7800 A/W. Above 110 μ W/cm², the responsivity decreases slightly to 2500 A/W at 1.5 mW/cm². This increase in responsivity with increasing incident power and subsequent saturation is consistent with previous reports of high gain GaN MSM photodetectors, 20 however, opposite of the trend seen in phototransistors. 13

Measurements of the transient response of the 2DEG-IDT device were conducted using Setup I with an optical chopper operating at 5 Hz. These measurements, presented in Figure 2c, demonstrate rise and fall times of 32 and 76 ms, respectively, here defined as the time it takes the photocurrent to go from 10% to 90% of its final value. It is also observed that within a 200 ms window, the photocurrent does not recover to

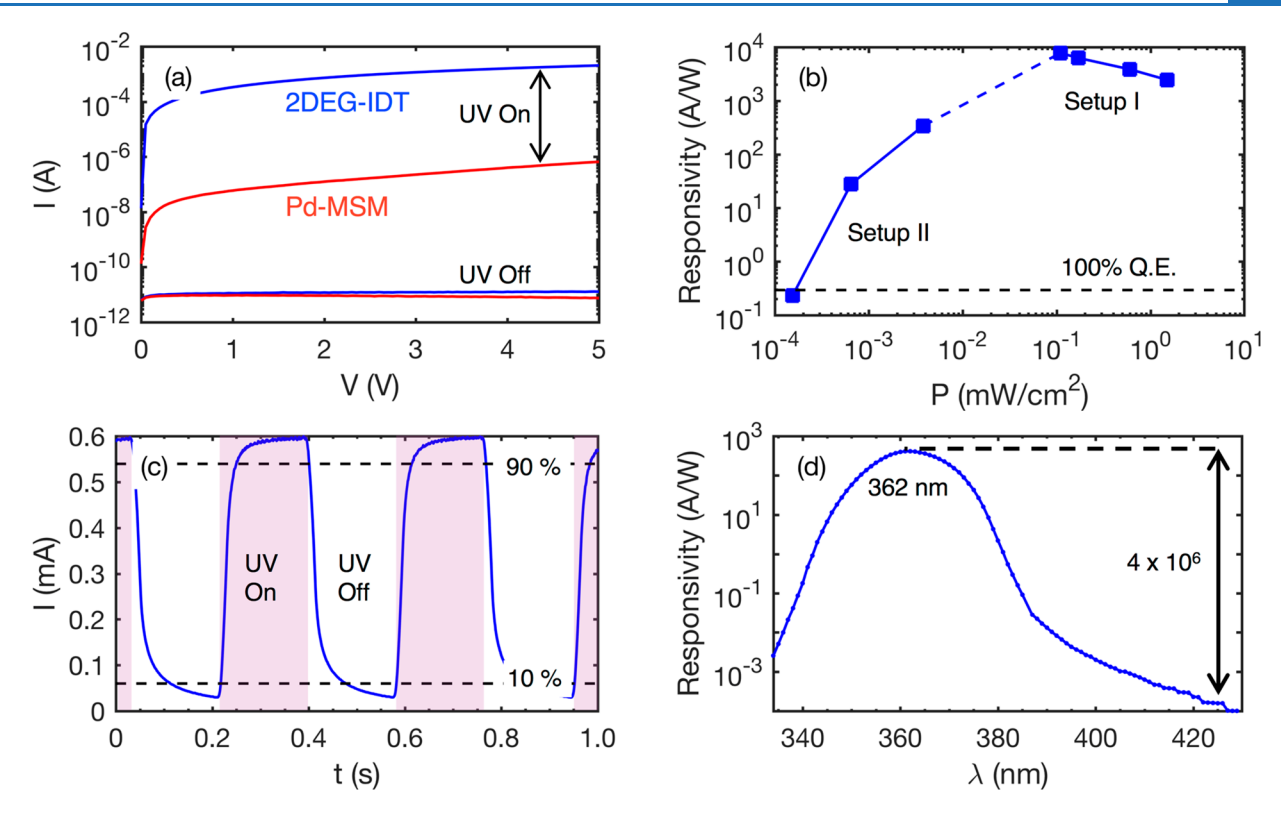


Figure 2. (a) UV photoresponse of characteristic 2DEG-IDT and MSM devices exposed to 1.5 mW/cm² UV power. (b) Responsivity as a function of incident power, with the responsivity corresponding to 100% Q.E. labeled. Measurements below 0.010 mW/cm² were performed using Setup II, and those above 0.010 mW/cm² were performed with Setup I. (c) Transient measurement of 2DEG-IDT response to 0.17 mW/cm² 365 nm illumination chopped at 5 Hz, measured in Setup I. (d) Responsivity vs wavelength, measured in Setup II. Measurements in (b), (c), and (d) were at a bias voltage of 5 V.

its ~10 pA dark state value, indicating the presence of persistent photoconductivity, common to AlGaN/GaN photodetector devices. ^{25,26} To investigate the role of surface traps in the transient response of our photodetector, 2DEG-IDT devices were cofabricated with a ~20 nm atomic layer deposited alumina (ALD-Al₂O₃) passivation layer, which has previously been shown to reduce the effect of surface traps on AlGaN/GaN device performance. ²⁷ Transient measurements of one such device are presented in Supporting Information, Figure S1, showing 30 ms/100 ms rise and fall times, comparable to the unpassivated devices. This insensitivity of the transient behavior of our photodetector to surface passivation indicates that surface traps do not significantly contribute to its transient behavior.

These measured rise and fall times are long relative to MSM photodetectors with no internal gain; however, they present a significant improvement on the 20 s rise and 60 s fall times observed in a photoconductor with comparable gain to our 2DEG-IDT device. He is well established that the response time of photoconductors and phototransistors scales with gain due to the accumulation of carriers leading to increased charging times. Thus, response times comparable to the 72 MHz bandwidth recently demonstrated in a GaN photodetector with subunity gain are fundamentally not achievable in a high gain photodetector such as our 2DEG-IDT device.

Measurements of responsivity as a function of wavelength were also performed using Setup II. These data, shown in Figure 2d, demonstrate a high UV-visible rejection ratio of 4 \times 10⁶, with a peak responsivity at ~362 nm. The broadband light source used in this measurement had a roughly constant intensity between 1 and 3 μ W/cm² below the peak

responsivity at 362 nm and an increasing intensity between 3 and $28 \ \mu W/cm^2$ as the wavelength increased from 362 to 430 nm (see Supporting Information, Figure S2). Because the responsivity of the 2DEG-IDT photodetector increases with incident power (as seen in Figure 2), this measurement underestimates the true UV–visible rejection ratio. The bandpass nature of the spectral responsivity of this photodetector, where the responsivity decreases at wavelengths both below and above the GaN band gap (\sim 365 nm), is consistent with previous reports of phototransistors, ^{13,19} indicating a similar gain mechanism in both devices.

We seek to explain the gain observed in both device architectures, in particular, the extraordinarily high gain of 26000 observed in the 2DEG-IDT. In order to understand the scaling laws of the gain mechanisms in MSM and 2DEG-IDT photodetectors, devices were fabricated where the intrinsic GaN channel length between the Pd and 2DEG electrodes was varied from 4 to 20 μ m. Optical microscope images of the MSM and 2DEG-IDT structures are shown in the insets of Figure 3a and b, respectively. Figure 3a,b shows the gain versus $1/L^2$, where L is the spacing between the Pd and 2DEG electrodes, respectively. These data show that while there is a clear linear relation, with zero y-intercept, between gain and 1/ L^2 for the 2DEG-IDT photodetectors (Figure 3b), the same relation does not describe the gain versus $1/L^2$ relation in the MSM photodetectors (Figure 3a). This difference in length scaling, in addition to the vastly different response magnitudes, implies that different gain mechanisms are present in these two types of devices.

In the standard model of gain in photoconductors, which has been used by Kumar et al.¹⁷ to describe the gain of an InAlN/

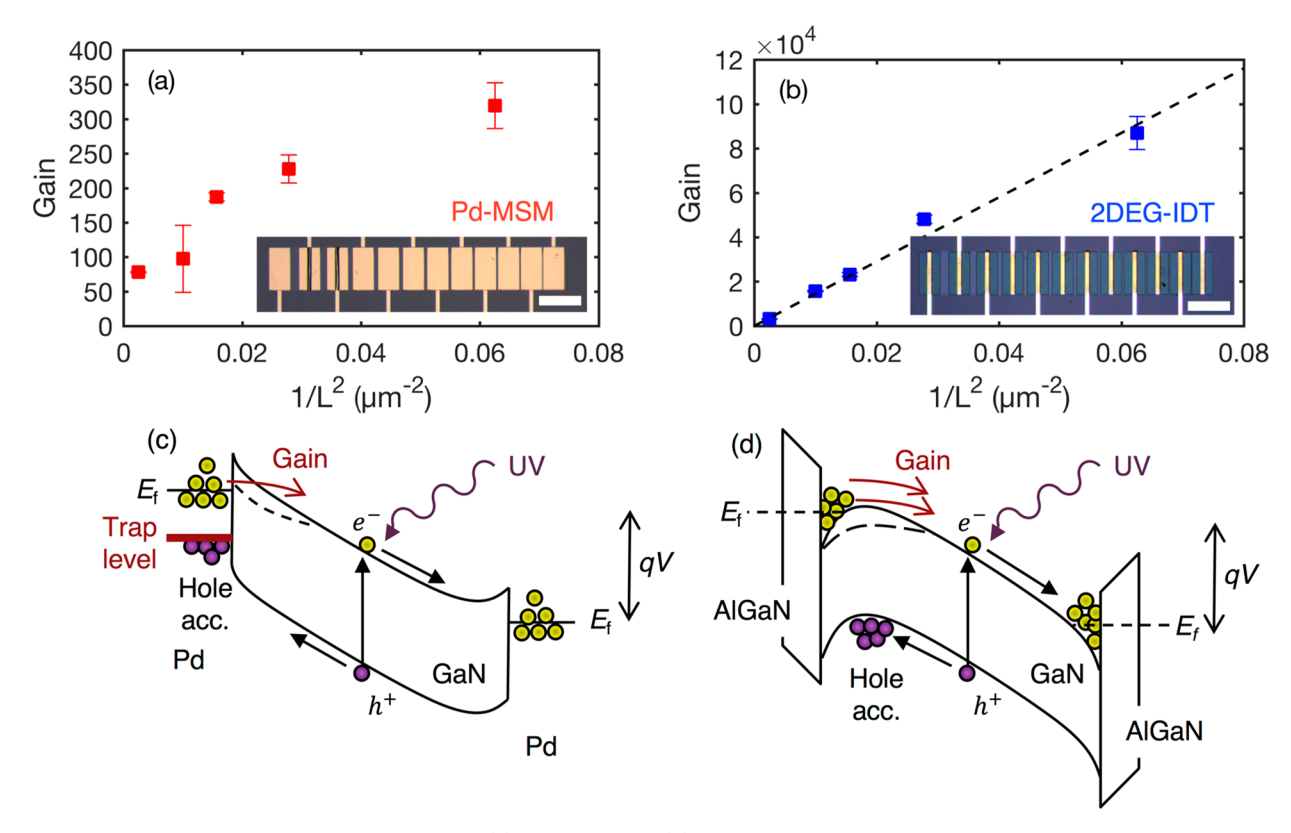


Figure 3. Comparison of internal gain vs length for (a) Pd-MSM and (b) 2DEG-IDT photodetectors. Error bars represent response biasing photodetector at ± 5 V. Insets show microscope images of fabricated devices with spacing of 4–20 μ m, scale bars represent 100 μ m. It is observed that there is a linear proportionality between gain and $1/L^2$ for the 2DEG-IDT device (black dashed line), but not for the Pd-MSM device. Band structures for the Pd-MSM and 2DEG-IDT photodetectors under applied bias are found in (c) and (d), respectively. Dashed lines in GaN conduction band represent electrostatic barrier lowering due to photon-induced hole accumulation.

GaN device with a similar architecture to this work, gain is due to carrier accumulation that is limited by recombination, leading to the following scaling law: $G = \mu_e \tau_r V/L^2$, where μ_e is the electron mobility, τ_r is the recombination time, and V is the applied voltage. Though this model reproduces the appropriate $1/L^2$ dependency, using a bulk mobility of 900 cm²/V·s, which is appropriate for our unintentional doping concentration, ²⁹ a recombination time of $\sim 3~\mu s$ is required to fit our data. This value is 3 orders of magnitude larger than the previously reported $\sim 6~ns$ minority carrier lifetimes in GaN. ³⁰ Because the $\sim 3~\mu s$ recombination time required to fit the standard model is unreasonable, a different gain mechanism is needed to describe the behavior of our 2DEG-IDT devices.

The proposed gain mechanism is schematically illustrated in the band diagram for a 2DEG-IDT photodetector presented in Figure 3d. In the 2DEG-IDT device, an AlGaN/GaN valence band offset creates an energetic barrier, which leads to hole accumulation at this interface. This hole accumulation leads to an electrostatic lowering of the energetic barrier for electrons in the 2DEG to escape the quantum well and enter the conduction band (dashed line in Figure 3d). Using only the lowermost sub-band, the number of carriers per unit volume with sufficient energy to escape the 2DEG quantum well can be approximately written as

$$n_{\rm e}(\phi_{\rm b}) \approx \frac{k_{\rm b}Tm^*}{\pi\hbar^2} \exp\left(-\frac{q(\phi_{\rm b} - \Delta\phi_{\rm b})}{k_{\rm b}T}\right)$$
 (2)

where m^* is the effective mass, $\phi_{\rm b}$ is the energy separation between the Fermi level in the 2DEG and the top of the GaN

conduction band in the dark state, and $\Delta\phi_b$ is the barrier lowering due to photon-induced hole accumulation (Figure 3d). Assuming that all electrons with sufficient energy enter the conduction band and that electron conduction between the 2DEG electrodes is due to drift, the gain is found to be

$$G = \frac{n_{\rm e}(\phi_{\rm b})}{n_{\rm ph,tot}} \frac{\mu_{\rm e} V}{L} \tag{3}$$

where $n_{\mathrm{ph,tot}}$ is the total number of photons incident on the device. Évidence for a drift model comes from the fact that the photocurrent shown in Figure 2a is approximately linear with applied voltage. This drift model can further explain the $1/L^2$ dependency of gain if $n_{\rm e}(\phi_{\rm b}) \propto F_{\rm ph}$, where $F_{\rm ph}$ is photon flux per unit area. Thus, because $n_{\rm ph,tot} = F_{\rm ph}L$, under this assumption, the gain can be rewritten as $G = n_e(\phi_b)\mu_e V/F_{ph}L^2$, reproducing the $1/L^2$ dependency. Using a mobility of 900 cm²/V·s, the barrier height required to explain the observed photocurrents is ~150 meV. This order of magnitude is consistent with theoretical values for $\phi_{\rm b}$, calculated to be ~100 meV using a commercial Schrödinger-Poisson solver.³¹ The exponential nature of the model in eq 2 further explains the observation in Figure 2b, where increasing incident power increases responsivity, up to a point of saturation. At low incident powers, when $\phi_{\rm b}$ – $\Delta\phi_{\rm b} \approx \phi_{\rm b}$, small changes in $\Delta\phi_{\rm b}$ lead to small changes in the number of conduction electrons. However, when $\phi_b - \Delta \phi_b$ is lowered at high incident powers, the same small change in $\Delta \phi_{\rm b}$ will lead to an exponentially larger change in the number of conduction electrons. This continues until reaching a point of saturation

where nonidealities, such as increased recombination in the channel and the AlGaN/GaN interface, lead to a divergence from this model. This gain mechanism is similar to that of a phototransistor, where minority carrier accumulation in the base lowers the base-emitter energetic barrier, allowing more majority carriers to be injected from the emitter.²¹

The band structure of an MSM photodetector, schematically illustrated in Figure 3c, has no barrier to hole conduction into the metal, in contrast to the 2DEG-IDT device. Thus, in order for spatial hole accumulation to occur, which is necessary to achieve a gain greater than unity, 32 a trap state must exist at the metal contact. The gain due to such a trap state would be limited by the density of trap states and the detrapping time, thus, the assumption $n_{\rm e}(\phi_{\rm b}) \propto F_{\rm ph}$ is unlikely to hold. This explains the fact that gain in the Pd-MSM photodetector is not linearly proportional to $1/L^2$. Though trap states could exist at the AlGaN/GaN interface, the difference in the scaling of the gain with length in these devices indicates that trap states do not play the same role in determining the gain of the 2DEG-IDT device as they do in the Pd-MSM device.

In conclusion, we demonstrated a 2DEG-IDT photodetector with a record high NPDR (6×10^{14}), in addition to a high responsivity (7800 A/W) and UV-visible rejection-ratio (10^6). The observed 32/76 ms rise/fall times present significant improvements on the 20/60 s rise/fall times seen in a photoconductor with comparable gain. We argue that the gain mechanism in this device is similar to that of a phototransistor, where spatial hole accumulation leads to a lowering of the energy barrier for electrons entering the conduction band. This mechanism is consistent with the scaling of gain with incident power and device channel length. The simple, two-mask fabrication process further allows for monolithic integration of our device with AlGaN/GaN HEMTs, enabling on-chip integration of optical sensing systems using this material platform.

METHODS

Setup I. We illuminate devices using a 6 W, 365 nm UV lamp (UVP, EL series UV lamp) and record photocurrent using a semiconductor parameter analyzer (Agilent B1500A). An UV light meter (SPER Scientific, Model 850009) was used to measure the incident UV intensity. The intensity was varied using a home-built chopper attached the UV lamp.

Setup II. We illuminate devices using low intensity broadband white light from a thermal light source and record photocurrent generated from the device across a range of photon wavelengths. The optical beam from the broadband thermal source (quartz halogen lamp) was directed through a monochromator (Acton Pro SP-2150i) and a mechanical chopper (200 Hz) onto the sample where it was focused down to a spot with a diameter larger than the 2DEG-IDT device. The photocurrent was measured by using a preamplifier (SRS-570) connected to a lock-in-amplifier (SRS-830), locked to the chopping frequency. A commercial silicon photodetector (Hamamatsu S1223) was used to calibrate the light intensity incident on the sample. We used a set of neutral density filters to vary the light intensity on the sample while keeping the chopping frequency fixed at 200 Hz.

ASSOCIATED CONTENT

S Supporting Information

The Supporting Information is available free of charge on the ACS Publications website at DOI: 10.1021/acsphotonics.8b01169.

Measurements of ALD-Al₂O₃ passivated 2DEG-IDT device and calibration curve for Setup II (PDF).

AUTHOR INFORMATION

Corresponding Author

*E-mail: dsenesky@stanford.edu.

ORCID 4

Ananth Saran Yalamarthy: 0000-0003-2734-0921

A. K. M. Newaz: 0000-0001-8159-1604

Author Contributions

[‡]These authors contributed equally to this work.

Notes

The authors declare no competing financial interest.

ACKNOWLEDGMENTS

This work was supported by the National Science Foundation (NSF) Engineering Research Center for Power Optimization of Electro Thermal Systems (POETS) under Grant EEC-1449548. N.A.S. and A.K.M.N. acknowledge the support from the National Science Foundation Grant ECCS-1708907. The devices were fabricated in the Stanford Nanofabrication Facility (SNF), which was partly supported by the NSF as part of the National Nanotechnology Coordinated Infrastructure (NNCI) under Award ECCS-1542152.

REFERENCES

- (1) Chen, H.; Liu, K.; Hu, L.; Al-Ghamdi, A. A.; Fang, X. New Concept Ultraviolet Photodetectors. *Mater. Today* **2015**, *18*, 493–502.
- (2) Monroy, E.; Omnès, F.; Calle, F. Wide-Bandgap Semiconductor Ultraviolet Photodetectors. Semicond. Sci. Technol. 2003, 18, R33.
- (3) Tsai, Y. L.; Lai, K. Y.; Lee, M. J.; Liao, Y. K.; Ooi, B. S.; Kuo, H. C.; He, J. H. Photon Management of GaN-Based Optoelectronic Devices via Nanoscaled Phenomena. *Prog. Quantum Electron.* **2016**, 49, 1–25.
- (4) Miller, R. A.; So, H.; Chiamori, H. C.; Suria, A. J.; Chapin, C. A.; Senesky, D. G. A Microfabricated Sun Sensor Using GaN-on-Sapphire Ultraviolet Photodetector Arrays. *Rev. Sci. Instrum.* **2016**, *87*, 095003.
- (5) Zheng, W.; Huang, F.; Zheng, R.; Wu, H. Low-Dimensional Structure Vacuum-Ultraviolet-Sensitive (λ < 200 Nm) Photodetector with Fast-Response Speed Based on High-Quality AlN Micro/Nanowire. *Adv. Mater.* **2015**, *27*, 3921–3927.
- (6) Zheng, W.; Lin, R.; Ran, J.; Zhang, Z.; Ji, X.; Huang, F. Vacuum-Ultraviolet Photovoltaic Detector. ACS Nano 2018, 12, 425–431.
- (7) Zheng, W.; Lin, R.; Zhang, D.; Jia, L.; Ji, X.; Huang, F. Vacuum-Ultraviolet Photovoltaic Detector with Improved Response Speed and Responsivity via Heating Annihilation Trap State Mechanism. *Adv. Opt. Mater.* **2018**, 1800697.
- (8) Chui, C. O.; Okyay, A. K.; Saraswat, K. C. Effective Dark Current Suppression with Asymmetric MSM Photodetectors in Group IV Semiconductors. *IEEE Photonics Technol. Lett.* **2003**, *15*, 1585–1587.
- (9) An, Y.; Behnam, A.; Pop, E.; Ural, A. Metal-Semiconductor-Metal Photodetectors Based on Graphene/p-Type Silicon Schottky Junctions. *Appl. Phys. Lett.* **2013**, *102*, 013110.
- (10) Chang, S.; Chang, M.; Yang, Y. Enhanced Responsivity of GaN Metal-Semiconductor-Metal (MSM) Photodetectors on GaN Substrate. *IEEE Photonics J.* **2017**, *9*, 6801707.

(11) Xu, G. Y.; Salvador, A.; Kim, W.; Fan, Z.; Lu, C.; Tang, H.; Morkoç, H.; Smith, G.; Estes, M.; Goldenberg, B.; et al. High Speed, Low Noise Ultraviolet Photodetectors Based on GaN p-i-n and AlGaN(p)-GaN(i)-GaN(n)Structures. *Appl. Phys. Lett.* **1997**, *71*, 2154.

- (12) Tut, T.; Gokkavas, M.; Inal, A.; Ozbay, E. Based Avalanche Photodiodes with High Reproducible Avalanche Gain $Al_xG_{1-x}N$ -Based Avalanche Photodiodes with High Reproducible Avalanche Gain. *Appl. Phys. Lett.* **2007**, *90*, 163506–253516.
- (13) Yang, W.; Nohava, T.; Krishnankutty, S.; Torreano, R.; McPherson, S.; Marsch, H. High Gain GaN/AlGaN Heterojunction Phototransistor. *Appl. Phys. Lett.* **1998**, *73*, 978–980.
- (14) Liu, L.; Yang, C.; Patanè, A.; Yu, Z.; Yan, F.; Wang, K.; Lu, H.; Li, J.; Zhao, L. High-Detectivity Ultraviolet Photodetectors Based on Laterally Mesoporous GaN. *Nanoscale* **2017**, *9*, 8142–8148.
- (15) Kahn, M. A.; Shur, M. S.; Chen, Q.; Kuznia, J. N.; Sun, C. J. Gated Photodetector Based on GaN/AlGaN Heterostructure Field Effect Transistor. *Electron. Lett.* **1995**, *31*, 398–400.
- (16) Martens, M.; Schlegel, J.; Vogt, P.; Brunner, F.; Lossy, R.; Würfl, J.; Weyers, M.; Kneissl, M. High Gain Ultraviolet Photo-detectors Based on AlGaN/GaN Heterostructures for Optical Switching. *Appl. Phys. Lett.* **2011**, *98*, 211114.
- (17) Kumar, S.; Pratiyush, A. S.; Dolmanan, S. B.; Tripathy, S.; Muralidharan, R.; Nath, D. N. UV Detector Based on InAlN/GaNon-Si HEMT Stack with Photo-to-Dark Current Ratio > 107. Appl. Phys. Lett. 2017, 111, 251103.
- (18) Alaie, Z.; Nejad, S. M.; Yousefi, M. H. Recent Advances in Ultraviolet Photodetectors. *Mater. Sci. Semicond. Process.* **2015**, 29, 16–55.
- (19) Lee, M. L.; Sheu, J. K.; Shu, Y. R. Ultraviolet Bandpass Al0.17 Ga0.83 NGaN Heterojunction Phototransitors with High Optical Gain and High Rejection Ratio. *Appl. Phys. Lett.* **2008**, 92, 053506.
- (20) Xie, F.; Lu, H.; Xiu, X.; Chen, D.; Han, P.; Zhang, R.; Zheng, Y. Low Dark Current and Internal Gain Mechanism of GaN MSM Photodetectors Fabricated on Bulk GaN Substrate. *Solid-State Electron.* **2011**, *57*, 39.
- (21) Sze, S. M.; Ng, K. K. Physics of Semiconductor Devices; John Wiley & Sons, Inc.: Hoboken, NJ, U.S.A., 2006.
- (22) Mireles, F.; Ulloa, S. E. Acceptor Binding Energies in GaN and AlN. Phys. Rev. B: Condens. Matter Mater. Phys. 1998, 58, 3879–3887.
- (23) Zaidi, Z. H.; Houston, P. A. Highly Sensitive UV Detection Mechanism in AlGaN/GaN HEMTs. *IEEE Trans. Electron Devices* **2013**, *60*, 2776–2781.
- (24) Hou, M.; Senesky, D. G. Operation of Ohmic Ti/Al/Pt/Au Multilayer Contacts to GaN at 600°c in Air. *Appl. Phys. Lett.* **2014**, *105*, 081905.
- (25) Hirsch, M. T.; Wolk, J. A.; Walukiewicz, W.; Haller, E. E. Persistent Photoconductivity in N-Type GaN. *Appl. Phys. Lett.* **1997**, 71, 1098–1100.
- (26) Katz, O.; Bahir, G.; Salzman, J. Persistent Photocurrent and Surface Trapping in GaN Schottky Ultraviolet Detectors. *Appl. Phys. Lett.* **2004**, 84, 4092–4094.
- (27) Hashizume, T.; Ootomo, S.; Hasegawa, H. Suppression of Current Collapse in Insulated Gate AlGaN/GaN Heterostructure Field-Effect Transistors Using Ultrathin Al2O3 Dielectric. *Appl. Phys. Lett.* **2003**, 83, 2952–2954.
- (28) Ho, K.-T.; Chen, R.; Liu, G.; Shen, C.; Holguin-Lerma, J.; Al-Saggaf, A. A.; Ng, T. K.; Alouini, M.-S.; He, J.-H.; Ooi, B. S. 32 Gigabit-per-Second Visible Light Communication Link with InGaN/GaN MQW Micro-Photodetector. *Opt. Express* **2018**, *26*, 3037.
- (29) Shur, M.; Gelmont, B.; Asif Khan, M. Electron Mobility in Two-Dimensional Electron Gas in AIGaN/GaN Heterostructures and in Bulk GaN. *J. Electron. Mater.* **1996**, *25*, 777–785.
- (30) Bandić, Z. Z.; Bridger, P. M.; Piquette, E. C.; McGill, T. C. Minority Carrier Diffusion Length and Lifetime in GaN. *Appl. Phys. Lett.* **1998**, *72*, 3166–3168.
- (31) Birner, S.; Zibold, T.; Andlauer, T.; Kubis, T.; Sabathil, M.; Trellakis, A.; Vogl, P. Nextnano: General Purpose 3-D Simulations. *IEEE Trans. Electron Devices* **2007**, *54*, 2137–2142.

(32) Dan, Y.; Zhao, X.; Mesli, A. A Photoconductor Intrinsically Has No Gain. 2015.